

# Evaluation of Core Heterogeneity Effect on Pulse-decay Experiment

Bao Jia, Jyun-Syung Tsau and Reza Barati  
University of Kansas

*This paper was prepared for presentation at the International Symposium of the Society of Core Analysts held in Vienna, Austria, 27 August -1 September 2017*

## ABSTRACT

Microcrack and heterogeneity are essential to tight oil and gas production, but there exists great uncertainty and challenge to evaluate them even at the core scale. Pulse-decay experiments are routinely used to measure petrophysical properties of tight cores. In this study, effects of permeability magnitude and location of the microcrack on pulse-decay experiments are numerically evaluated based on our experimental scenarios. The simulation model is three dimensional with dual permeability and concentrates the fracture in the middle of the core. Permeability value of the core in each grid is populated homogeneously and heterogeneously, and different correlation lengths are used to describe the spatial distribution patterns.

Pulse-decay experiments are performed on a tight carbonate core by flowing helium in both forward and reverse directions under different pressures. A preferential flow path is discovered even when the microcrack is not present in a tight core. We suggest that very early pressure response in a pulse-decay experiment should be closely examined to identify the preferential flow path, and failure to identify the preferential flow path leads to significant porosity and permeability underestimation.

## INTRODUCTION

Table 1 chronologically lists representative work of exploring petrophysical properties using pulse-decay method since 1968. Among them the work by Kamath et al. (1992), Ning (1992), Cronin (2014) and Alnoaimi (2016) are highlighted for this study as they explored heterogeneity/microcrack related petrophysical properties. Kamath et al. (1992) combined two separate cores with different values of permeability and flowed water through them from forward and reverse directions. They evidenced qualitatively that the pressure responses are direction dependent, implying that heterogeneity plays a role affecting the pulse-decay experiment. They also demonstrated the dual porosity phenomenon in a fractured core. Ning (1992) analytically and numerically explored the dual porosity and dual permeability phenomenon in a fractured core. Cronin (2014) proposed a layered simulator to continuously study effects of heterogeneity and fracture on the pressure response in a pulse-decay experiment. Alnoaimi (2016) performed pulse-decay experiments in fractured shales using helium and carbon dioxide, and made efforts to history match the pressure curves.

Authors	Contributions
Brace et al. (1968)	Firstly applied pulse-decay method to measure permeability of granite
Lin (1977)	Put forward the basic numerical model for pulse-decay process
Hsieh et al. (1981)	Presented complete and restrictive analytical solution for pulse-decay process
Dicker and Smits (1988)	Simplified the complete analytical solution with acceptable accuracy
Kamath et al. (1992)	Characterized heterogeneity and microcrack of synthetic cores using pulse-decay method
Ning (1992)	Explored dual porosity and dual permeability of fractured cores analytically and numerically
Jones (1997)	Proposed valuable recommendations for pulse-decay experimental set-up design, for example, using cores with large diameter and short length
Cui et al. (2009)	Extended the flowing fluid from non-adsorptive gas to adsorptive gas
Civan (2010), Civan et al. (2010)	Incorporated other important variables in the numerical settings of pulse-decay
Cronin (2014)	Numerically explained impacts of anisotropy and microcrack on pulse-decay pressure response
Alnoaimi (2016)	Numerically matched pressure curves of non-adsorptive gas and adsorptive gas during a pulse-decay experiment
Jia et al. (2017a)	Comprehensively investigated flow behaviors of adsorptive and non-adsorptive gas in a wide range of pressure in a tight core using pulse-decay method

Table 1 Representative work regarding pulse-decay method in tight cores

In the light of the previous work, we constructed a three dimensional, dual permeability numerical model to demonstrate clearly how the permeability magnitude and different location of the microcrack in a tight core, and how the permeability heterogeneity and spatial distribution patterns affect pressure responses in a typical pulse-decay experiment. Kamath et al. (1992) investigated heterogeneity effect by flowing water and combing two separate cores, and in this work we use one core and flow gas from both the forward and reverse directions to observe the different flow behaviors. During the course of the experiment a preferential flow path is discovered in a natural heterogeneous core sample even a microcrack not present. We suggest the very early beginning of pressure response reveals the preferential flow path, and it should be emphasized in a general pulse-decay experiment.

## Procedure

Fig. 1 shows the pulse-decay experimental set-up. It is mainly composed of four components: first upstream reservoir  $U_1$ , second upstream reservoir  $U_2$ , core holder and downstream reservoir  $D$ . To investigate properties of a tight core under a certain pore pressure, one needs to inject gas into the system by constant pressure with valves  $V_1$  and  $V_2$  opened, and  $V_3$  closed. Subsequently, a pressure pulse is introduced into  $U_1$  with  $V_2$  closed. Finally after  $V_2$  is opened and  $V_1$  closed, the upstream pressure starts to decline and the downstream pressure rise. Analyzing these two pressure curves enables one obtain petrophysical properties of the core sample.

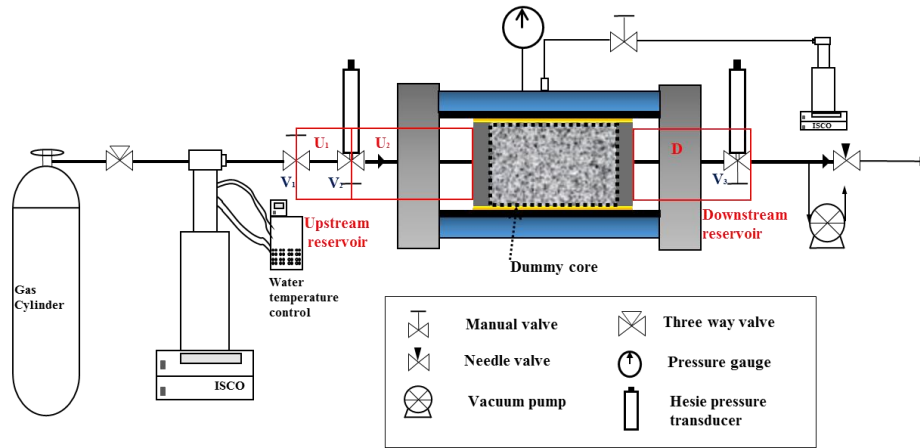


Fig. 1 Pulse-decay experimental set-up

Based on the experimental scenarios, a three dimensional model is constructed to numerically evaluate effects of microcrack and heterogeneity on the pressure response. Table 2 lists the details of the numerical setting of the core. A commercial reservoir simulator is used in this study (IMEX, 2015). The circular section is squared with the same cross-sectional area. The fracture is located in the fifth layer of the core.

length, cm	5.08	grid number	16*8*8
width, cm	3.38	porosity, fraction	0.02
grid size, cm	0.32*0.42*0.42	matrix permeability, mD	0.1

Table 2 Numerical setting for the core

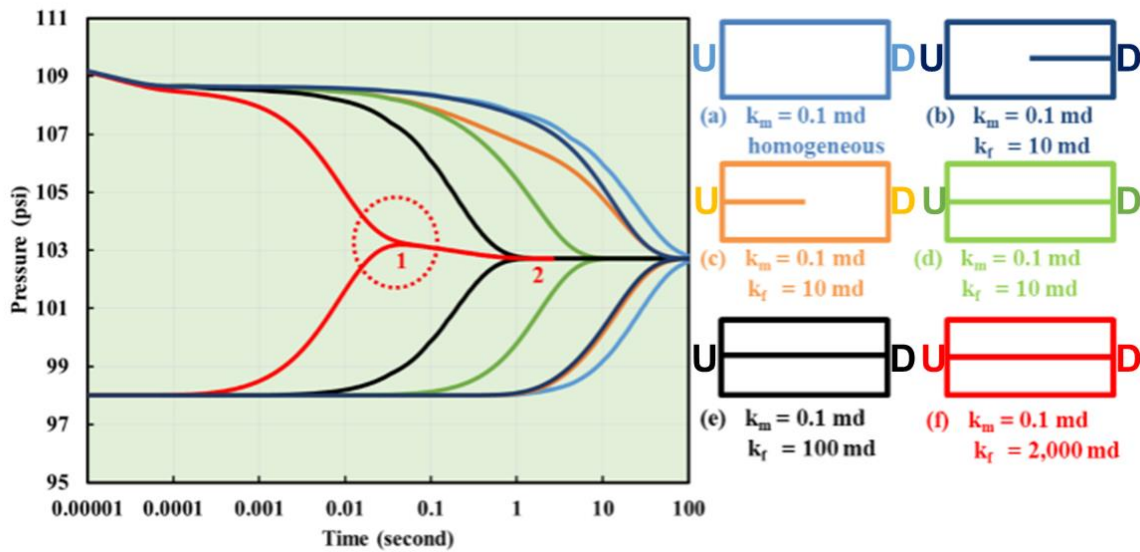


Fig. 2 Comparison of upstream and downstream pressure responses in six different core model configuration (a) homogeneous core with permeability of 0.1 mD (b) heterogeneous core with fracture of 10 mD at the rear half of the core (c) heterogeneous core with fracture of 10 mD at the front half of the core (d) heterogeneous core with fracture of 10 mD throughout the core (e) heterogeneous core with fracture of 100 mD throughout the core (f) heterogeneous core with fracture of 2,000 mD throughout the core. U represents upstream and D represents downstream.

Initially the core is saturated with helium and the downstream reservoir is maintained at 98 psi. A 10% of the initial pressure pulse was applied in the upstream reservoir. One homogeneous and five heterogeneous simulation scenarios are constructed to observe the impact of the microcrack. Fig. 2 plots pressure curves in the upstream and downstream in the six scenarios. An abrupt pressure decrease is observed at the very beginning as gas expands freely from the first upstream reservoir to the second upstream reservoir. Comparing the homogeneous scenario (a) and heterogeneous scenarios shows fracture expedites gas flow process, which is as expected. Comparing (b) and (c) shows that upstream pressure is sensitive to the microcrack location but downstream pressure is not. Upstream pressure curve in (c) declines much faster than that in (b), but downstream pressure curves come closest to coinciding in shape between (b) and (c). When permeability of the fracture increases to 10 mD and 100 mD in scenario (d) and (e), respectively, less time is required for the gas pressure in the upstream and downstream to reach equilibrium with a more permeable microcrack. As the permeability of microcrack increases to 2,000 mD, a “hump” region (red dashed circle) is formed before final pressure equilibrium (Alnoaimi, 2016). This behavior is caused by the “flow back” phenomenon (Fig. 3). Gas in the fracture travels faster and arrives at the downstream earlier than in the matrix, causing a “pseudo” equilibrium pressure at point 1 (Fig.2) when upstream pressure curve and downstream pressure curve converge. Afterwards gas in the downstream starts to flow back towards the upstream direction, and pressure continues to decrease until reaching the final equilibrium pressure at point 2 (Fig. 2).

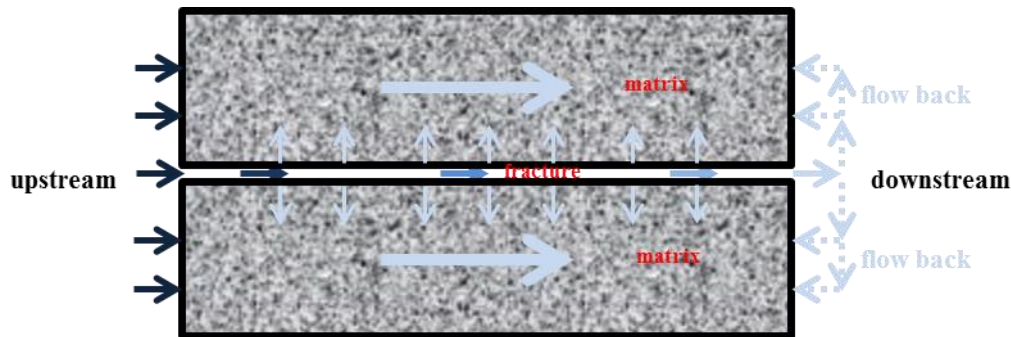


Fig. 3 Flow back phenomenon if a microcrack is present in the core.

Comparing (d), (e) and (f) reveals that, to identify a microcrack in a typical pulse-decay experiment, the difference of permeability between matrix and fracture must be large enough. After performing a series of sensitivity analysis by changing reservoir volume and pressure pulse size, two approaches are suggested to help identify the microcrack if the permeability difference is small: one is to reduce the reservoir volume and the other one is to reduce pressure pulse size. Actually, Kamath et al. (1992) experimentally concluded that using small vessels helps detect core heterogeneity. It is worthwhile to notice that, if a steady-state method is used to measure the permeability, the result should be independent of the microcrack location, as the permeability is calculated based on the total pressure drop across the core.

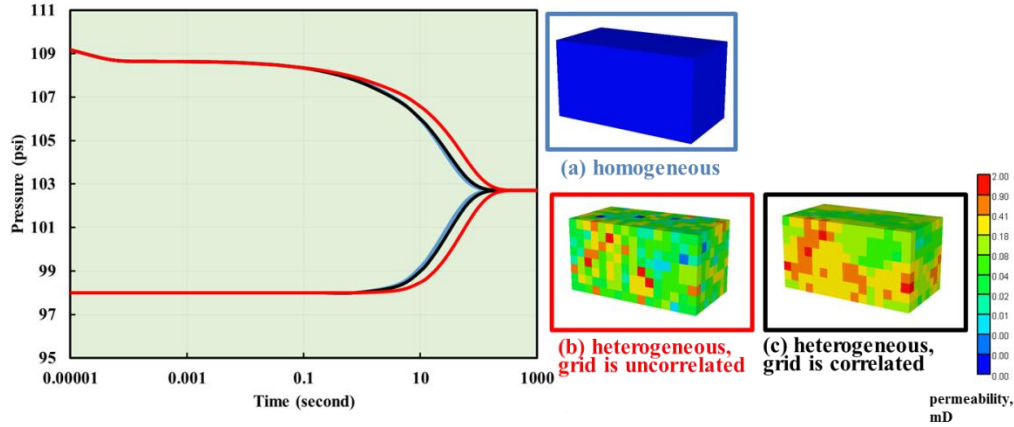


Fig. 4 Comparison of pressure response in upstream and downstream of the core in three simulation scenarios (a) homogeneous core with permeability of 0.1 mD (b) heterogeneous core with correlation length of one grid size (c) heterogeneous core with correlation length of the width of the cross section.

Subsequent simulations investigate effects of heterogeneity and correlation length on pressure responses if a microcrack is not present in the core. Permeability distribution is generated geostatistically by Stanford Geostatistical Modeling Software (SGeMS) (Remy et al. 2009). Mean value is 0.1 mD in all the simulation scenarios shown in Fig. 4, and the heterogeneity degree of heterogeneous scenarios, evaluated by Dykstra-Parsons coefficient, is the same. In this figure, (a) is homogeneous, (b) is heterogeneous, but each grid is not correlated, which means the correlation length is set as the grid size (0.32 cm). (c) and (b) share the same permeability values quantitatively implies that the degree of heterogeneity is the same, but their permeability distributions are different. Correlation length in (c) is the width of the cross section (3.38 cm).

Comparing (a) and (b) shows that, more time is needed to reach pressure equilibrium in the heterogeneous scenario, implying that heterogeneity hampers the gas flow process in the porous media. This difference is caused by the energy dissipation occurring along the flow path when the porous media is heterogeneous. However, as the correlation length is increased in scenario (c), time to reach pressure equilibrium is close to that of the homogeneous scenario, implying that a longer correlation length reduces energy dissipation and favors gas flow if the degree of heterogeneity is the same. Therefore, the core behaves similar to the more permeable scenario.

A series of pulse decay test was conducted on a tight carbonate core, of which the pore size distribution was analyzed with nuclear magnetic resonance (NMR) spectroscopy.

Two relaxation time are involved in NMR: T1 and T2. T1 is longitudinal relaxation time and T2 is spin relaxation time. Both T1 and T2 are important for characterizing PSD, but T2 measurement is much faster, thus it is more practical (Arnold 2007).

$$\frac{1}{T_{2A}} = \frac{1}{T_{2F}} + \frac{1}{T_{2S}} + \frac{1}{T_{2D}} \quad (1)$$

In equation (1), the subscript A, F, S, D denote apparent, free fluid, surface-induced, and diffusion-induced respectively. Free fluid relaxation time is several seconds, but T1 and

T2 are of several milliseconds, thus the free fluid term could be ignored. In heterogeneous local magnetic fields, the diffusion-induced term contribution is negligible. Therefore, equation (1) could be approximated as

$$\frac{1}{T_{2A}} \approx \frac{1}{T_{2S}} \quad (2)$$

The surface-induced term equals

$$\frac{1}{T_S} = \rho_2 \frac{S}{V} \quad (3)$$

Where  $\rho_2$  is surface relaxivity related to mineral surfaces properties (e.g. iron(III) content), the value is estimated to be 5 ~ 30  $\mu\text{m/s}$  for mudstone and sandstones, and 0.15 ~ 3.6  $\mu\text{m/s}$  for carbonate, and the value applied to generate the pore size distribution in this study is 1  $\mu\text{m/s}$ . S is surface area and V is volume. If the grain is assumed to be spherical, the ratio of surface area and volume could be correlated with diameter d as follow:

$$d = \frac{6}{S/V} \quad (4)$$

Thus, the reciprocal of the relaxation time equals:

$$\frac{1}{T_2} = \rho_2 \frac{6}{d} \quad (5)$$

Figure 5 presents the size distribution of the core which ranges from 0.6 nm to 6 nm peaking at about 1.3 nm. Porosity obtained from the NMR is 0.037.

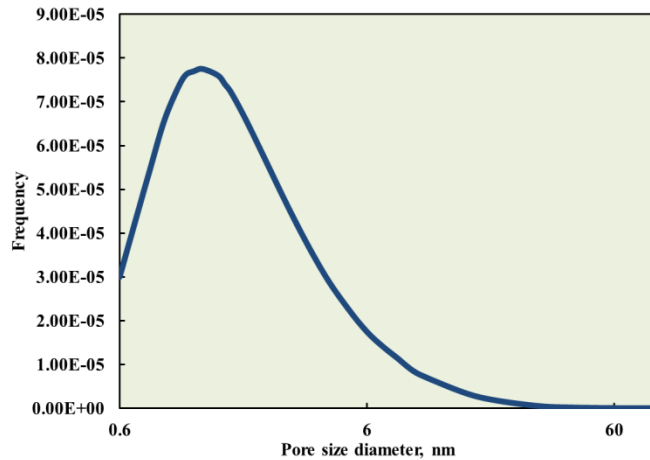


Fig. 5 Pore size distribution by NMR.

Fig. 6 shows entire pressure curves in a pulse decay experiment. Initially, core sample and downstream are saturated with helium under pressure of 98 psi ( $p_d$ ), and the first upstream reservoir is saturated with helium under pressure of 110.1 psi ( $p_u$ ). Valve V1 is opened at the 10th second. Helium expands freely to the second upstream reservoir and flows into the core inlet. Heise pressure transducers in this set-up record data points every second. Upstream reservoir pressure drops abruptly at the 11th second. It firstly drops to a lowest point and then increases slightly to 106.6 psi ( $p'_u$ ) due to the Joule-Thomson effect. At the

same time, pressure response in the downstream is also observed. The downstream pressure is increased to 98.3 psi ( $p'_d$ ).

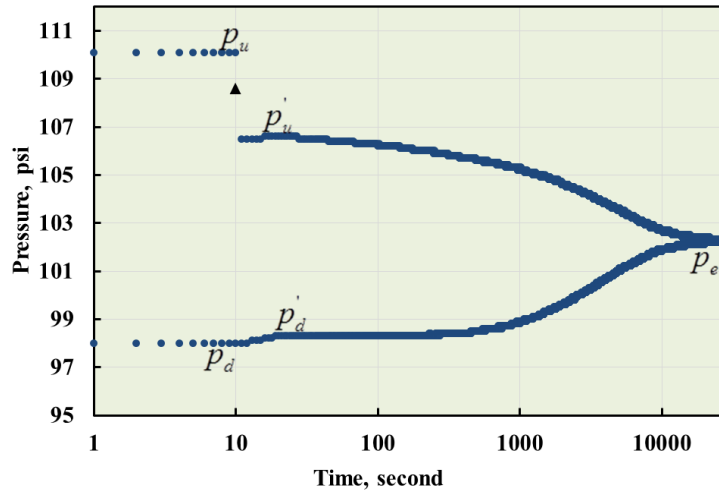


Fig. 6 Pressure data points in estimating total porosity and secondary accessible porosity in a pulse-decay experiment

$$\frac{p_u V_{u1}}{Z_u} + \frac{p_d (V_{u2} + V_p + V_d)}{Z_d} = \frac{p_e (V_{u1} + V_{u2} + V_p + V_d)}{Z_e} \quad (6)$$

$$\frac{p'_u (V_{u1} + V_{u2})}{Z_u} + \frac{p'_d (V_p + V_d)}{Z_d} = \frac{p_e (V_{u1} + V_{u2} + V_p + V_d)}{Z_e} \quad (7)$$

	$p_u$	$p_d$	$p'_u$	$p'_d$	$p_e$
pressure, psi	110.1	98	106.6	98.3	102.3
compressibility factor, Z	1.0040	1.0036	1.0039	1.0037	1.0038

Table 3 Pressure and compressibility factor of data points in Fig. 6.

Two methods using Boyle's law are employed to calculate porosity. Equation (6) is formed based on the pressure of  $p_u$ ,  $p_d$  and  $p_e$ , and equation (7) is formed based on the pressure of  $p'_u$ ,  $p'_d$  and  $p_e$ ,  $V_{u1}$ ,  $V_{u2}$  and  $V_d$  are volumes of the first upstream reservoir, second upstream reservoir and downstream reservoir, and the values are 3.147 cm<sup>3</sup>, 0.431 cm<sup>3</sup> and 3.183 cm<sup>3</sup>, respectively. Table 3 lists the corresponding compressibility factor under the specific pressure and 86 °F.  $V_p$  and  $V'_p$  are pore volumes estimated by the two equations. Ideally, for a homogeneous core, porosity values estimated from equation (6) and (7) should be the same. However, noticeable difference exists between the two values. As we are dealing with very small volumes of the reservoir, the result might be misleading even if the measured volume of the reservoir deviates slightly from the real value. To validate our results, a dummy core with zero porosity is placed inside the core holder, in order to measure the reduced pressure after opening valve  $V_1$ . This pressure is marked with black triangle in Fig. 6, and it is compared with the result estimated using our measured volumes of the first upstream and second upstream reservoir. This step ensures the accuracy of our test result.

Based on the pressure responses during the test, we suggest that the preferential flow path exists in a natural, tight and heterogeneous core even if a microcrack is not present. Gas will choose different flow paths through the core from upstream to downstream. The flow path is preferential if it is less tortuous and with higher permeability. On the other hand, the flow path is described as the secondary flow path when the tortuosity increases and permeability decreases. We examined closely the pressure curves throughout the experiment and found that gas flow in the preferential flow path occurs at the very beginning of the pulse-decay experiment, which finishes within one second based on our observation, and it is much faster than in the secondary flow path. Thus, the concepts of total and secondary accessible porosity, estimated from equation (6) and (7), respectively, are proposed in this work to differentiate the two types of flow path.

Prior to the constant pressure injection, vacuuming is applied to excavate air in the system as the flowing gas is helium in tests. Then constant pressure gas injection from the ISCO pump is performed until the final pressure equilibrium is obtained in the system. Fig. 7 plots upstream and downstream pressures during this process. Unlike the scenario that pore space is already under a certain level of pressure, no pressure response occurs instantaneously at the downstream reservoir as a constant pressure is exerted at the upstream, even though the pressure pulse is more than 100 psi. This observation implies that the preferential flow path forms in the tight porous media only when gas has fully saturated the core.

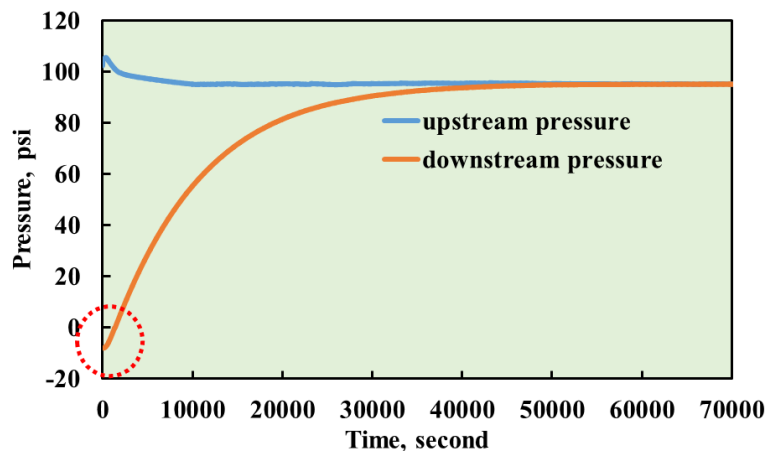


Fig. 7 Constant pressure gas injection to form gas saturation in the pulse-decay set-up.

Subsequent tests are performed by continuously increasing the pore pressure. The effective stress is kept constant at 2,000 psi by controlling the confining pressure. After reaching the pore pressure of approximately 300 psi, pressure in the system is relieved and the core sample is reverted and placed in the core holder to repeat the experiment under the same pressure. Fig. 8 shows two types of porosity calculated from the test at different pressures. Significant difference exists between the total porosity and secondary accessible porosity during the pressure range from 100 psi to 300 psi. Total porosity is approximately 0.035 for both forward and reverse directions. Secondary accessible porosity is approximately 0.012 and 0.025 in the forward and reverse directions, respectively, the difference is because  $p'_u$  is lower in the forward direction, which is caused by the heterogeneity

characteristic of the core. Moreover, the fact that  $p'_u$  is lower in the forward direction actually reveals that the front half of the core is more permeable than the rear half of the core.

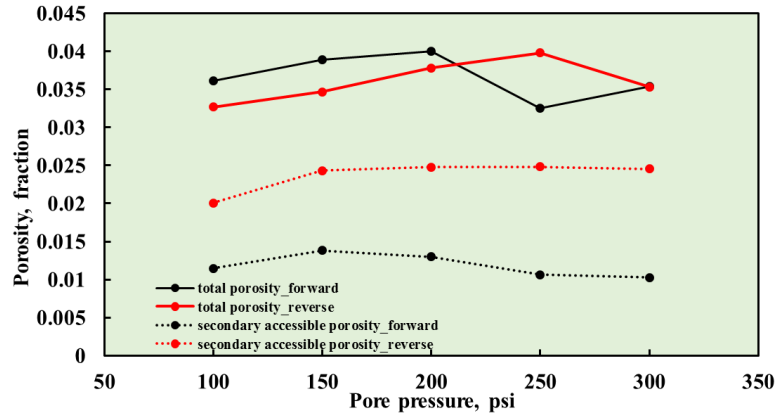


Fig. 8 Total porosity and secondary accessible porosity in the core in the forward and reverse directions.

Fig. 9 shows experimental and simulated pressure curves under the initial pore pressures approximately of 100 psi, 150 psi, 200 psi, 250 psi and 300 psi of flowing gas from the forward and reverse directions. The simulating process requires initial pressures in the upstream and downstream, reservoir volumes, core configuration including diameter, length and porosity. Permeability value is finely tuned in the simulator to history match experimental curves, the matched permeability is apparent permeability of the porous media taking into account of the non-Darcy flow behavior occurred in tight porous media, including slip flow and Kundsén diffusion. Surface diffusion will also occur if the flowing gas is adsorptive. Sensitivity analysis was performed using various grids number, and the result shows that the pressure curves are insensitive to the grids number in the model. Using the matched permeability values, simulated pressure curves are also plotted as in forward/reverse directions in Fig. 9. In this work, no specific optimization algorithm is developed to obtain permeability value, thus the matched permeability is an approximation. Matched permeability value is very close in the forward and reverse directions, and the difference is within 20 nD which is negligible compared with the total value, thus, the permeability as a function of pressure is represented as one value, as shown in Fig. 10. Dummy core pressure tests referred previously for each pore pressure further validates the accuracy of our measured reservoir volumes.

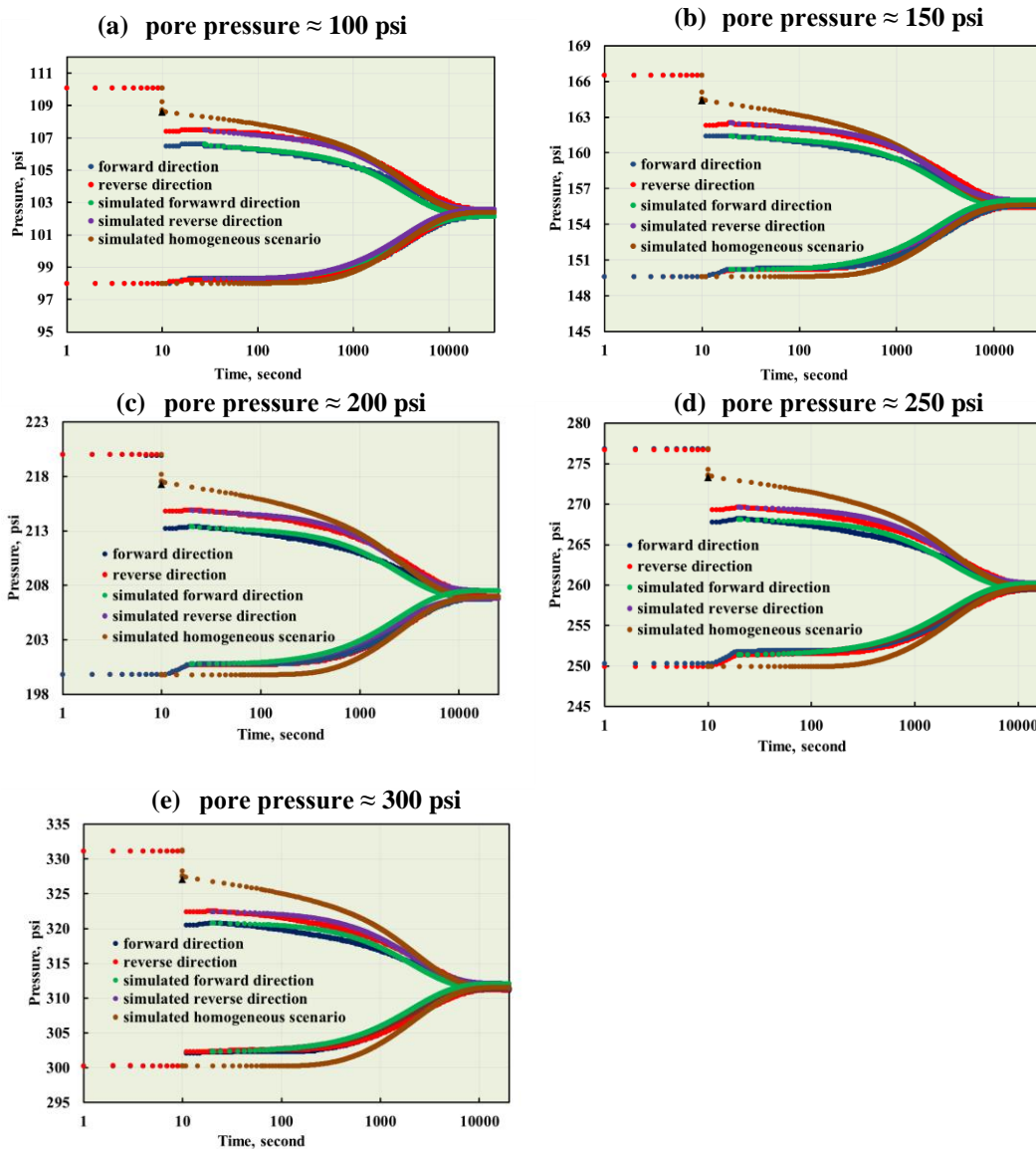


Fig. 9 Experimental and simulated pressure curves in the pulse-decay experiment. Experiment results include pressure curves by flowing helium in the forward and reverse directions, pressure ranges from 100 psi to 300 psi (from (a) to (e)). Pressure curve is adjusted within  $\pm 0.2$  psi for better visualization of comparing pressure responses in different directions. The black triangle point is the experimental reduced pressure after gas freely expands from the first upstream reservoir to the second upstream reservoir if a dummy core replaces the natural core sample. Simulated pressure curves are generated by matching the late-time pressure response using the secondary accessible porosity, and the homogeneous scenarios are constructed based on the averaged permeability obtained from the matching results using the total porosity.

Fig. 10 also shows the first order Klinkenberg equation to describe the slip flow behavior, where  $k_{\infty}$  is intrinsic permeability of the porous media and  $b$  is slip factor describing the degree of permeability deviation from Darcy's law. Matched permeability varies from 600 nD to 400 nD under the pore pressures ranging from 100 psi to 300 psi. Gas behaves more permeable under low pressure due to the slip flow and Knudsen diffusion behavior (Jia et al. 2017b).

$$k = k_{\infty} \left(1 + \frac{b}{p}\right) \quad (7)$$

Using the matched permeability, an idealized homogeneous scenario is simulated starting from the initial pressure  $p_u$  and  $p_d$ . Thus the three sets of simulated pressure curves share the same permeability and reach the final equilibrium pressure almost at the same time. However, as the permeability in the preferential flow path must be much larger than that in the secondary flow path, as the pressure decrease in the preferential finishes within one second. We could reasonably infer that purely estimating permeability starting at  $p'_u$  and  $p'_d$  significantly underestimates both porosity and permeability.

The preferential flow path is more important under a higher pressure. As pore pressure increases, larger deviation of  $p'_u$  from the reduced pressure using the dummy core is observed, which is the value should be obtained if the core is homogeneous. More rapid response is observed at the downstream, as the difference between  $p'_d$  and  $p_d$  becomes more pronounced and the time for  $p_d$  to reach  $p'_d$  is shorter. For example, in the 300 psi scenario, 300.2 psi increases to 302.3 psi within only one second.

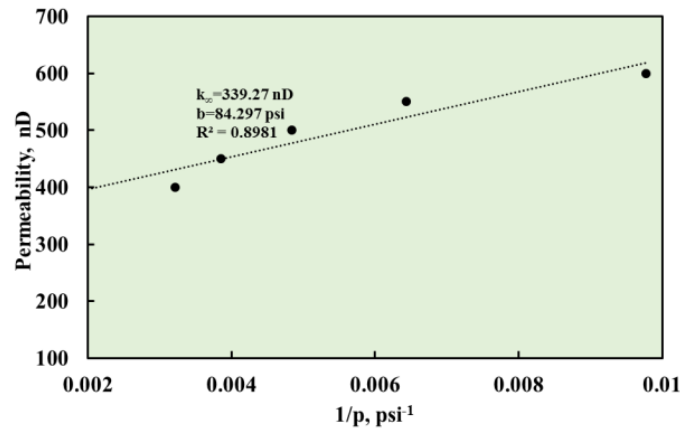


Fig. 10 Permeability as a function of  $1/p$ .

The permeability curve in Fig. 10 behaves a downward curvature, which is unlike the result of steady-state permeability measurements. This phenomenon is also observed by Lenormand et al. (2010) and Rushing et al. (2004), which is more evident in more permeable core samples. This effect is due to the non-Darcy flow effects, mainly slip flow caused by the non-slip boundary condition and inertial flow in the transient flow regime.

The effect of the preferential path on permeability discussed in this study might be confirmed by experimental tracer tests. Gas can be applied if the permeability is too low. In addition, simulation of tracer tests on the heterogeneous scenarios might also be helpful. These can be next research focuses of this subject.

## Conclusions

The following conclusions are obtained from this study:

- A microcrack can be detected by the pulse-decay experiment when it causes a “hump” region.

- The preferential flow path exits in a natural, tight and heterogeneous core even when microcrack is not present.
- Gas flows through the preferential flow path at the very early beginning. Failing to take the early pressure response into account leads to significant underestimation of porosity and permeability.
- The formation of a preferential flow path in heterogeneous porous media is more pronounced under an elevated pore pressure.
- In a typical pulse-decay experiment, the upstream reservoir pressure is sensitive to the core heterogeneity but the downstream reservoir pressure is not.
- Performing a pulse-decay experiment in both the forward and reverse directions assists differentiating which part of the core is more permeable.

### Acknowledgements

The authors are grateful to the financial support from Tertiary Oil Recovery Program (TORP) at the University of Kansas, the technical support from Mr. Scott Ramskill, the NMR data provided by Fan Zhang, and Professor Chi Zhang in geology department in the University of Kansas, and the core sample from Kansas Geological Survey,.

### REFERENCES

1. Alnoaimi, K. R. 2016. Influence of Cracks and Microcracks on Flow and Storage Capacities of Gas Shales at Core-level. Ph.D. thesis, Stanford University.
2. Arnold, J. 2007. Mobile NMR for Rock Porosity and Permeability. Ph.D. thesis, RWTH Aachen University.
3. Brace, W. F., Walsh, J. B., and Frangos, W. T. 1968. Permeability of Granite under High Pressure. *Journal of Geophysical Research* **73** (6): 2225-2236. <http://doi.org/10.1029/JB073i006p02225>.
4. IMEX. IMEX user's guide-version. Canada: Computer Modelling Group, Ltd; 2015.
5. Civan, F. 2010. A Review of Approaches for Describing Gas Transfer through Extremely Tight Porous Media, AIP Conference Proceedings, Montecatini, Italy, 20-25 June. <http://doi.org/10.1063/1.3453838>.
6. Civan, F., Rai, C. S., and Sondergeld, C. H. 2010. Intrinsic Shale Permeability Determined by Pressure-Pulse Measurements Using a Multiple-Mechanism Apparent-Gas-Permeability Non-Darcy Model, SPE Annual Technical Conference and Exhibition, Florence, Italy, 19-22 September. SPE-135087-MS. <http://doi.org/10.2118/135087-MS>.
7. Cronin, M. B. 2014. Core-scale Heterogeneity and Dual-Permeability Pore Structure in the Barnett Shale. Master thesis, University of Texas at Austin
8. Cui, X., Bustin, A. M. M., and Bustin, R. M. 2009. Measurements of Gas Permeability and Diffusivity of Tight Reservoir Rocks: Different Approaches and Their Applications. *Geofluids* **9** (3): 208-223. <http://doi.org/10.1111/j.1468-8123.2009.00244.x>.
9. Dicker, A. I., and Smits, R. M. 1988. A Practical Approach for Determining Permeability From Laboratory Pressure-Pulse Decay Measurements, International Meeting on Petroleum Engineering, Tianjin, China, 1-4 November. SPE-17578-MS. <http://doi.org/10.2118/17578-MS>.

10. Hsieh, P. A., Tracy, J. V., Neuzil, C. E., Bredehoeft, J.D., and Silliman, S.E. 1981. A transient Laboratory Method for Determining the Hydraulic Properties of 'Tight' Rocks—I. Theory. *International Journal of Rock Mechanics and Mining Sciences & Geomechanics Abstracts* **18** (3): 245-252. [http://doi.org/10.1016/0148-9062\(81\)90979-7](http://doi.org/10.1016/0148-9062(81)90979-7).
11. Jia, B., Tsau, J., and Barati, R. 2017. Different Flow Behaviors of Low-pressure and High-pressure CO<sub>2</sub> in Shales, Unconventional Resources Technology Conference, Austin, Texas, USA, 24-26 July. URTEC-2690239-MS. <http://doi.org/10.15330-URTEC-2017-2690239>.
12. Jia, B., Li, D., Tsau, J., and Barati, R. 2017. Gas Permeability Evolution During Production in the Marcellus and Eagle Ford Shales: Coupling Diffusion/Slip-flow, Geomechanics, and Adsorption/Desorption, Unconventional Resources Technology Conference, Austin, Texas, USA, 24-26 July. URTEC-2695702-MS. <http://doi.org/10.15330-URTEC-2017-2695702>.
13. Jones, S. C. 1997. A Technique for Faster Pulse-Decay Permeability Measurements in Tight Rocks. *SPE Formation Evaluation* **12** (01): 19-26. <http://doi.org/10.2118/28450-PA>.
14. Kamath, J., Boyer, R. E., and Nakagawa, F. M. 1992. Characterization of Core Scale Heterogeneities Using Laboratory Pressure Transients. *SPE Formation Evaluation*: **7** (03) 219-227. <http://doi.org/10.2118/20575-PA>.
15. Lenormand, R., Bauget, F., Ringot, G. 2010. Permeability Measurement on Small Rock Samples, International Symposium of the Society of Core Analysts, Halifax, Nova Scotia, Canada, 4-7 October. SCA2010-32.
16. Lin, W. 1977. Compressible Fluid Flow through Rocks of Variable Permeability, Lawrence Livermore Laboratory, Livermore, California.
17. Ning, X. 1992. The Measurement of Matrix and Fracture Properties in Naturally Fractured Low Permeability Cores Using a Pressure Pulse Method. Ph.D. thesis, Texas A&M University.
18. Remy, N., Boucher, A., and Wu, J. 2009. Applied geostatistics with SGeMS: A user's guide. Cambridge, UK: Cambridge University Press.
19. Rushing, J. A., Newsham, K. E., Lasswell, P. M., Cox, J. C., Blasingame T. 2004. Klinkenberg-Corrected Permeability Measurements in Tight Gas Sands: Steady-State Versus Unsteady-State Techniques, SPE Annual Technical Conference and Exhibition, Houston, Texas, USA, 26–29 September. SPE-89867-MS. <https://doi.org/10.2118/89867-MS>.